

# Puncture Evolution of Schwarzschild Black Holes

J. David Brown

*Department of Physics, North Carolina State University, Raleigh, NC 27695 USA*

The moving puncture method is analyzed for a single, non-spinning black hole. It is shown that the puncture region is not resolved by current numerical codes. As a result, the geometry near the puncture appears to evolve to an infinitely long cylinder of finite areal radius. The puncture itself actually remains at spacelike infinity throughout the evolution. In the limit of infinite resolution the data never become stationary. However, at any reasonable finite resolution the grid points closest to the puncture are rapidly drawn into the black hole interior by the  $\Gamma$ -driver shift condition. The data can then evolve to a stationary state. These results suggest that the moving puncture technique should be viewed as a type of “natural excision”.

With the moving punctures technique, vacuum black holes are modeled on a numerical grid with  $\mathbb{R}^3$  topology. The interior of each black hole contains an asymptotic region that is represented as a point or “puncture” where the gravitational field diverges. To be precise, the initial data are chosen to be conformally flat,  $g_{ab} = \psi^4 \tilde{g}_{ab}$ , where  $\tilde{g}_{ab}$  is the flat metric in Cartesian coordinates. The conformal factor  $\psi$  behaves like  $1/r$  at each puncture where  $r$  is the coordinate distance from the puncture point. The numerical grid is constructed in such a way that the punctures do not coincide with any grid point. The initial data are evolved with the BSSN formulation of the evolution equations [1, 2] along with “1+log” slicing,

$$\frac{\partial \alpha}{\partial t} = \beta^a \partial_a \alpha - 2\alpha K, \quad (1)$$

and the  $\Gamma$ -driver shift condition,

$$\frac{\partial \beta^a}{\partial t} = \frac{3}{4} B^a, \quad (2a)$$

$$\frac{\partial B^a}{\partial t} = \frac{\partial \tilde{\Gamma}^a}{\partial t} - \eta B^a. \quad (2b)$$

Here,  $\alpha$  is the lapse function,  $\beta^a$  is the shift vector, and  $K$  is the trace of the extrinsic curvature. The conformal connection functions are defined by  $\tilde{\Gamma}^a \equiv -\partial_b \tilde{g}^{ab}$  with  $\det(\tilde{g}_{ab}) = 1$ . Variants of these gauge conditions are obtained by dropping the advection term  $\beta^a \partial_a \alpha$  in Eq. (1) or replacing one or more of the time derivatives in Eqs. (2) by  $\partial/\partial t - \beta^a \partial_a$ . [3, 4]

The moving puncture method was discovered through careful numerical experimentation [5, 6] and has been applied successfully by a number of groups. (See, for example, Refs. [4, 7, 8, 9, 10, 11, 12, 13].) Recent analytical and numerical work on single, nonspinning (Schwarzschild) black holes was carried out with the purpose of clarifying how the geometry evolves in the neighborhood of a puncture. [14, 15] These works focus on the behavior of the numerical slices in a three-dimensional evolution code, and find that the puncture evolves from a  $\psi \sim 1/r$  singularity to a  $1/\sqrt{r}$  singularity as the space-like slice evolves to a stationary state. Because the physical metric behaves like  $\psi^4(dr^2 + r^2 d\Omega)$  with  $\psi \sim 1/\sqrt{r}$

near the puncture point  $r = 0$ , the geometry represents a three-dimensional “cylinder” of infinite proper length and finite areal radius. Stationary foliations with these properties have been described numerically and analytically. [14, 16, 17]

The purpose of this report is to extend these insights. I show that the time required for the puncture to evolve to a  $1/\sqrt{r}$  singularity increases with increasing resolution. In the limit of infinite resolution the puncture would retain its  $1/r$  character throughout any finite-time evolution. The behavior of the puncture that is seen in numerical studies can be misleading because the puncture region is not resolved.

The geometrical picture of puncture evolution that is presented here applies to a single, nonrotating black hole. It is not clear whether the same description applies to black holes with spin and linear momentum. For puncture initial data the conformal factor diverges like  $1/r$  at each puncture. [18] This suggests that initially, the evolution of the geometry near each puncture point will be independent of the spin and momentum. As the conformal factor changes, the geometry in the vicinity of a puncture could develop a dependence on spin and momentum.

The discussion will be presented using the notation and terminology of the Kruskal–Szekeres diagram, shown in Fig. 1. [19] The Kruskal–Szekeres diagram represents the maximal analytic extension of a Schwarzschild black hole.

The black hole interior is region II, and we live in the asymptotically flat exterior region I. Region III is the “other” asymptotically flat region, separated from I by a wormhole. The heavy curves are the future and past singularities. The axes  $u$  and  $v$  are Kruskal–Szekeres coordinates in which the metric reads

$$ds^2 = \frac{32M^3}{R} e^{-R/2M} (-dv^2 + du^2) + R^2 d\Omega^2. \quad (3)$$

Each point in the  $u$ - $v$  plane is a sphere of areal radius  $R$ , where  $R$  is defined by

$$u^2 - v^2 = \left( \frac{R}{2M} - 1 \right) e^{R/2M}. \quad (4)$$

The lines at  $\sim 45^\circ$  are the horizons with  $R = 2M$ . The areal radius is greater than  $2M$  in the exterior regions I

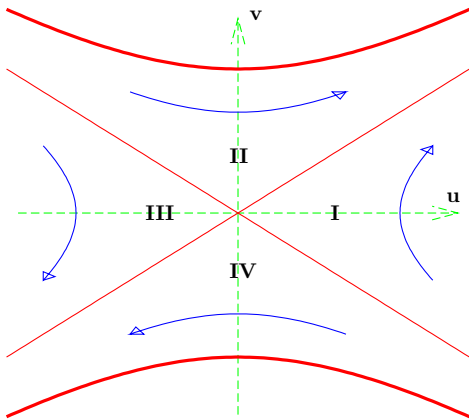


FIG. 1: Kruskal-Szekeres diagram of a Schwarzschild black hole.

and III. The areal radius is less than  $2M$  in regions II and IV.

The curved arrows in Fig. 1 show the directions of a Killing vector field, which is taken as future pointing in our region I. Note that any slice can be extended to a stationary foliation by Lie transport along the Killing vector field. In the Hamiltonian or 3+1 language, any spacelike slice can be evolved into a time-independent history if the lapse and shift are chosen such that the time flow vector field  $t^\mu \equiv \alpha n^\mu + \beta^\mu$  coincides with the Killing vector field. (Here,  $n^\mu$  is the unit timelike normal to the slices and  $\beta^\mu$  is the shift vector expressed as a spacetime vector field.) Note that we cannot have a stationary foliation with  $\alpha > 0$  everywhere if the slices extend into both regions I and III. The foliations found in Refs. [14, 16, 17] are examples of stationary foliations that begin in region II and end in region I, extending from  $u \sim -\infty, v \sim \infty$  to  $u \sim \infty, v \sim \text{finite}$ . For any such foliation whose slices asymptotically approach an  $R = \text{const}$  curve in region II (a hyperbola in Kruskal-Szekeres coordinates), the slice geometries will approach that of an infinitely long three-dimensional cylinder. The stationary foliation found in Refs. [16, 17] satisfies the maximality condition  $K = 0$ , while the stationary foliation discussed in Ref. [14] satisfies the stationary “1+log” slicing condition  $2\alpha K = \beta^a \partial_a \alpha$ .

The initial data for puncture evolution of a Schwarzschild black hole consist of the spatial metric in isotropic coordinates,

$$ds^2 = (1 + M/(2r))^4 (dr^2 + r^2 d\Omega^2), \quad (5)$$

and vanishing extrinsic curvature. These are the data for the  $v = 0$  slice of the Kruskal-Szekeres diagram. For the initial data the relationship between  $u$  and the isotropic radial coordinate  $r$  is given by

$$u = \frac{1}{2} \left( \sqrt{\frac{2r}{M}} - \sqrt{\frac{M}{2r}} \right) \exp \left[ \frac{1}{8} \left( \sqrt{\frac{2r}{M}} + \sqrt{\frac{M}{2r}} \right)^2 \right]. \quad (6)$$

The positive  $u$  axis is covered by  $M/2 \leq r < \infty$  and the negative  $u$  axis is covered by  $0 < r \leq M/2$ . Initially the puncture point  $r = 0$  coincides with spacelike infinity in region III,  $u = -\infty$ .

The key question is this. Can the initial data  $v = 0$  evolve to a slice that begins in region II and ends in region I? The answer is no. We can see this most clearly by keeping in mind that, in Hamiltonian language, the momentum constraint is the generator of spatial diffeomorphisms. As a consequence the time derivatives in the 3+1 evolution equations appear only in the combination  $\partial_\perp \equiv \partial/\partial t - \mathcal{L}_\beta$ , where  $\mathcal{L}_\beta$  is the Lie derivative along the shift vector  $\beta^a$ . Let us assume that the slicing condition has this same property: time derivatives appear only in the combination  $\partial_\perp$ . When this is the case, the evolution equations and slicing condition together determine the history of the (intrinsic and extrinsic) geometry of space. The lapse function specifies the point wise proper time separation between instances of space (or “slices”) at successive times. The choice of shift vector does not affect the spatial geometry. The role of the shift vector is to determine how the spatial coordinates are carried from one slice to the next. In a finite difference calculation the shift vector determines how the distribution of grid points is carried from one slice to the next.

Consider the evolution of the initial geometry represented by the  $v = 0$  slice using 1+log slicing, Eq. (1). We can ignore how the grid points are distributed initially, and how they are redistributed in time by the shift vector. Now observe that the maximally extended Schwarzschild black hole is symmetric under reflections about the Kruskal-Szekeres  $v$  axis. Thus, the initial metric expressed in Kruskal-Szekeres coordinates (the metric of Eq. (3) with  $v = 0$ ) is invariant under  $u \rightarrow -u$ . The initial metric expressed in isotropic coordinates Eq. (5) is invariant under  $r \rightarrow M^2/(4r)$ . This reflection symmetry implies that the initial spatial geometry in region III is identical to the initial spatial geometry in region I. As long as the initial choice of lapse function is also reflection symmetric, then the geometry will remain symmetric as it evolves in time. If the part of the slice that extends to spatial infinity in region I does not evolve into region II, then the part of the slice that extends to spatial infinity in region III also does not evolve into region II.

In fact, neither end of the initial data slice  $v = 0$  can evolve entirely into the black hole interior (region II) in finite time. To see why this is the case, consider a sequence of spacelike slices whose members are separated by finite proper time, and whose initial slice is  $v = 0$ . Starting from a fixed point in region III on the initial slice, we can define a timelike trajectory of finite proper length that is orthogonal to each of the slices. Now take the limit as the fixed initial point moves to spacelike infinity. A timelike trajectory cannot extend from spacelike infinity to the black hole interior in finite proper time. This is clear from the Penrose diagram [19], which shows that a curve connecting spacelike infinity to the black hole interior must be null or somewhere spacelike. It fol-

lows that the timelike trajectory remains in region III. The spacelike slices must also extend into region III.

The argument above shows that the puncture point, which begins at spacelike infinity in region III, must remain in region III throughout its evolution. All of the slices evolved from  $v = 0$  begin in region III and end in region I. With a positive lapse these slices cannot reach a stationary state.

These results are confirmed by numerical tests. The tests described below are carried out with a BSSN code that assumes spherical symmetry. The code is based on a generalization of the BSSN formulation that does not assume  $\det(\tilde{g}_{ab}) = 1$ . [20] The evolved data include the components  $\tilde{g}_{rr}$  and  $\tilde{g}_{\theta\theta}$  of the conformal metric, the “chi version” of the conformal factor  $\chi \equiv 1/\psi^4$ , the trace of the extrinsic curvature  $K$ , the component  $\tilde{A}_{rr}$  of the trace-free part of the extrinsic curvature, and the conformal connection function  $\tilde{\Gamma}^r$ . The lapse function  $\alpha$  is determined by the 1+log slicing condition Eq. (1). Each of these variables, along with the shift vector component  $\beta^r$ , is a function of time  $t$  and radial coordinate  $r$ . The initial metric is given in Eq. (5). The finite difference grid is cell centered with grid points  $r_j = (j - 1/2)\Delta r$  for  $j = 1, 2, \dots$ . The puncture is located at  $r = 0$ . The code also tracks the Kruskal–Szekeres coordinates  $u$  and  $v$  of each grid point; this allows the slices to be displayed in a Kruskal–Szekeres or Penrose diagram. Further details of the 1-D code are described in Ref. [21].

Figure 2 shows the slice at time  $t = 3M$  as a curve just below the future singularity on the Kruskal–Szekeres diagram. The slice begins in region III and ends in region I. This slice was obtained by evolving the initial data  $v = 0$  with initial lapse function  $\alpha = 1$ . For this simulation the shift vector was set to zero for all time. The reflection symmetry about the  $v$ -axis is evident. The heavy dots in Fig. 2 show the locations of grid points obtained from a second simulation, identical to the first except for the use of the  $\Gamma$ -driver shift condition. For clarity of presentation only every other grid point is displayed, beginning with grid point  $j = 2$ . The resolution used for both of these runs was  $\Delta r = M/50$ ; this is comparable to the highest resolutions used in current 3D codes.

With the  $\Gamma$ -driver shift, the left-hand side of the Kruskal–Szekeres diagram is almost completely devoid of grid points by  $t = 3M$ . The asymmetry in the distribution of grid points occurs for two reasons. First, the grid points in the initial data are distributed uniformly in  $r$ , not in  $u$ . With an outer boundary at, say,  $100M$ , only 0.5% of the grid points start in the left half of the Kruskal–Szekeres diagram. Second, with the  $\Gamma$ -driver condition the shift vector quickly develops  $\beta^r \sim r$  behavior near the puncture. Since the conformal factor diverges like  $1/r$ , the magnitude of the shift vector behaves like  $\sqrt{\beta^r \psi^4 \tilde{g}_{rr} \beta^r} \sim 1/r$ . Due to its large magnitude at small  $r$ , the shift vector quickly drives the grid points in region III toward the black hole interior.

The spherically symmetric code differs from current three-dimensional black hole codes in one important re-

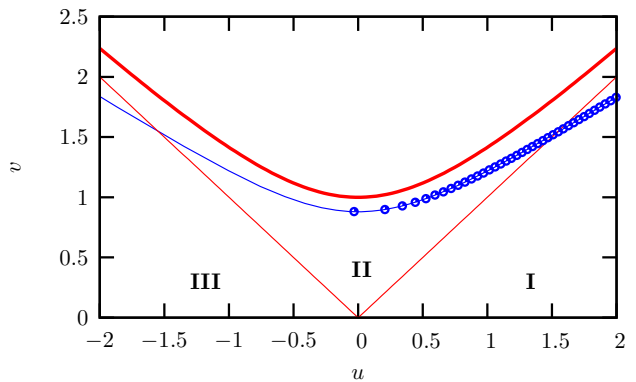


FIG. 2: Slice at  $t = 3M$  for vanishing shift (solid curve) and  $\Gamma$ -driver shift (dots).

spect: with the spherically symmetric code the puncture point  $r = 0$  is a boundary of the computational domain. In most contexts, the choice of boundary conditions will affect the evolution of the fields in the bulk. For puncture evolution, however, the results are found to be insensitive to the choice of boundary conditions at  $r = 0$ . This is most likely due to that fact that, with the  $\Gamma$ -driver shift condition, the grid points near the puncture quickly acquire superluminal speeds as they are drawn into the black hole interior. The grid points continue to evolve along spacelike trajectories that approximate the orbits of the Killing vector field. It follows that at the boundary  $r = 0$  all of the physical characteristics are directed from interior to exterior (toward the left in the Kruskal–Szekeres diagram). As a result one would not expect conditions imposed at  $r = 0$  to influence the evolution of the geometry.

With the spherically symmetric code we can easily increase the resolution well beyond the value used in the simulations of Fig. 2. This is an effective way to counteract the sparsity of grid points in region III in the initial data. For example, with  $\Delta r = M/50$  and the outer boundary at  $100M$  there are only 25 grid points with initial values  $u < 0$ . We can increase this by a factor of ten or more and still maintain reasonably short run times. However, a straightforward increase in resolution is not very effective in counteracting the movement of grid points caused by the  $\Gamma$ -driver shift condition. At resolutions as high as  $\Delta r = M/6400$  the shift vector still drives all of the grid points into the black hole interior within a time of a few  $M$ . See Fig. 3. After all of the grid points have left region III, the lapse and shift can settle into a stationary state where the time flow vector field  $t^\mu = \alpha n^\mu + \beta^\mu$  coincides with the Killing vector field.

For higher resolutions the time required for all of the grid points from region III to be driven into the black hole interior increases, as seen in Fig. 3. In the limit of infinite resolution, the grid points at any finite time would stretch from region III to region I, crossing the black hole interior like the curve in Fig. 2. At infinite resolution the

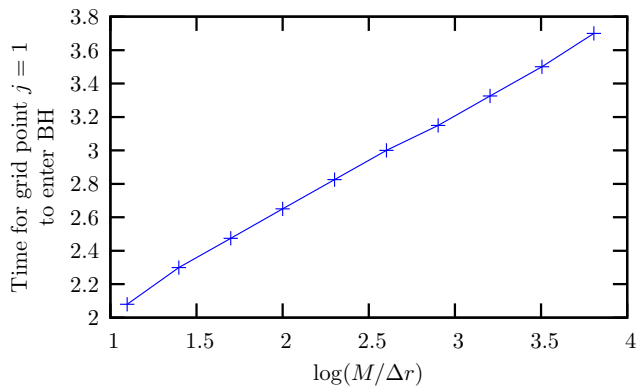


FIG. 3: The vertical scale is the time required (in units of  $M$ ) for all of the grid points that begin in region III to evolve into the black hole interior, region II, with the  $\Gamma$ -driver shift condition. The horizontal scale is the common logarithm of  $M/\Delta r$ . The resolutions used for this graph differ by powers of 2, ranging from  $\Delta r = M/12.5$  to  $\Delta r = M/6400$ .

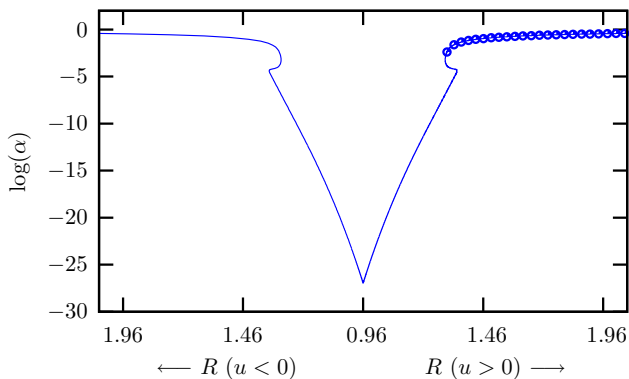


FIG. 4: Logarithm of the lapse  $\alpha$  as a function of areal radius  $R$  (in units of  $M$ ) at time  $t = 30M$  for vanishing shift (solid curve) and  $\Gamma$ -driver shift (dots).

slices never reach a stationary state. However, the time  $T$  required for the region III grid points to evolve into region II increases very slowly with resolution, roughly like  $T/M \sim 0.58 \log(M/\Delta r) + 1.5$ . We can compare this to the time scale for the lapse and shift to settle to a stationary state—at resolutions typical of current codes this is about  $50M$ . According to the heuristic expression for

$T/M$ , an extraordinarily high resolution of  $\Delta r \sim M/10^{83}$  would be required for grid points to remain in region III beyond  $t \sim 50M$ .

One of the important properties of the 1+log slicing condition is that the lapse function is driven to zero in the black hole interior, so the slices naturally avoid the physical singularity. Figure 4 shows the common logarithm of the lapse at time  $t = 30M$  plotted as a function of areal radius for both  $u > 0$  (right half of the graph) and  $u < 0$  (left half of the graph). The continuous curve was obtained from a simulation with vanishing shift vector and resolution  $\Delta r = M/800$ . The dots were obtained from a simulation with the  $\Gamma$ -driver shift condition and resolution  $\Delta r = M/50$ . (For clarity, only every other grid point is displayed.) Again we see that the evolution of the complete slice is symmetric under reflections  $u \rightarrow -u$ , but for the simulation with  $\Gamma$ -driver shift the distribution of grid points is highly asymmetric.

With the moving puncture method the region inside the black hole horizon is not completely resolved. As a matter of principle, the puncture point remains at space-like infinity in region III throughout its evolution. However, with the  $\Gamma$ -driver condition the shift vector quickly drives all of the region III grid points into the black hole interior. The resulting slices are incomplete; the grid points terminate in region II due to lack of resolution. The lapse function and shift vector adjust to bring the data to a stationary state. The stationary state is a portion of a slice that extends from  $u \sim -\infty$ ,  $v \sim \infty$  in region II to  $u \sim \infty$ ,  $v \sim \text{finite}$  in region I.

The lack of resolution that characterizes the puncture method is not likely to cause problems for finite difference codes at any reasonable resolution. In fact, the results here suggest that puncture evolution should be viewed as a type of “natural excision”. With black hole excision one intentionally removes from the computational domain a set of grid points inside the horizon (see, for example, Ref. [22]). In the case of puncture evolution the removal of grid points occurs naturally. The advantage over the traditional excision method is that puncture evolution does not require the introduction of an interior boundary where boundary conditions and special finite difference stencils must be applied.

I would like to thank Mark Hannam, Pablo Laguna, Niall O’Murchadha and Bernard Whiting for helpful discussions. This work was supported by NSF grant PHY-0600402.

[1] M. Shibata and T. Nakamura, Phys. Rev. **D52**, 5428 (1995).  
[2] T. W. Baumgarte and S. L. Shapiro, Phys. Rev. **D59**, 024007 (1999), gr-qc/9810065.  
[3] J. R. van Meter, J. G. Baker, M. Koppitz, and D.-I. Choi, Phys. Rev. **D73**, 124011 (2006), gr-qc/0605030.  
[4] B. Brügmann, J. González, M. Hannam, S. Husa, and U. Sperhake (2006), gr-qc/0610128.

[5] M. Campanelli, C. O. Lousto, P. Marronetti, and Y. Zlochower, Phys. Rev. Lett. **96**, 111101 (2006), gr-qc/0511048.  
[6] J. G. Baker, J. Centrella, D.-I. Choi, M. Koppitz, and J. van Meter, Phys. Rev. Lett. **96**, 111102 (2006), gr-qc/0511103.  
[7] F. Herrmann, D. Shoemaker, and P. Laguna (2006), gr-qc/0601026.

- [8] U. Sperhake (2006), gr-qc/0606079.
- [9] J. A. Gonzalez, U. Sperhake, B. Bruegmann, M. Hannam, and S. Husa, Phys. Rev. Lett. **98**, 091101 (2007), gr-qc/0610154.
- [10] M. Campanelli, C. O. Lousto, Y. Zlochower, B. Krishnan, and D. Merritt, Phys. Rev. **D75**, 064030 (2007), gr-qc/0612076.
- [11] J. G. Baker, S. T. McWilliams, J. R. van Meter, J. Centrella, D.-I. Choi, B. J. Kelly, and M. Koppitz (2006), gr-qc/0612117.
- [12] J. Thornburg, P. Diener, D. Pollney, L. Rezzolla, E. Schnetter, E. Seidel, and R. Takahashi (2007), gr-qc/0701038.
- [13] W. Tichy and P. Marronetti (2007), gr-qc/0703075.
- [14] M. Hannam, S. Husa, D. Pollney, B. Brügmann, and N. O’Murchadha (2006), gr-qc/0606099.
- [15] M. Hannam, S. Husa, B. Brügmann, J. González, U. Sperhake, and N. O’Murchadha (2006), gr-qc/0612097.
- [16] F. Estabrook, H. Wahlquist, S. Christensen, B. DeWitt, L. Smarr, and E. Tsiang, Phys. Rev. **D7**, 2814 (1973).
- [17] T. W. Baumgarte and S. G. Naculich (2007), gr-qc/0701037.
- [18] S. Brandt and B. Brügmann, Phys. Rev. Lett. **78**, 3606 (1997), gr-qc/9703066.
- [19] C. W. Misner, K. S. Thorne, and J. A. Wheeler, *Gravitation* (Freeman, 1973).
- [20] J. D. Brown, Phys. Rev. **D71**, 104011 (2005), gr-qc/0501092.
- [21] J.D. Brown, arXiv:0705.3845 [gr-qc].
- [22] M. Alcubierre, B. Brügmann, P. Diener, F. Herrmann, D. Pollney, E. Seidel, and R. Takahashi (2004), gr-qc/0411137.